Predictions for p+Pb Collisions at the LHC

R. Vogt

Lawrence Livermore National Laboratory, Livermore, CA 94551, USA
Physics Department, University of California, Davis, CA 95616, USA

with members and friends of the JET Collaboration

Contributions from: Javier Albacete *et al.* (rcBK, charged hadrons), Nestor Armesto (jets), Kari Eskola (π^0), Rainer Fries (direct photons), Vasile Topor Pop *et al.* (HIJING $\mathrm{B\overline{B}}$), Boris Kopeliovich ($R_{p\mathrm{Pb}}$ for produced pions), Kryzstof Kutak (azimuthal difference between jets), Gergeley Barnafoldi *et al.* (cold matter effects on charged hadrons), Amir Rezaeian (charged hadrons, pions, photons), Ivan Vitev (charged hadrons, π^0, photons), Xin-Nian Wang (charged hadrons), Ben-Wei Zhang (jets, gauge bosons), Ziwei Lin (AMPT predictions)

Caveats

Thanks to everyone who sent in predictions

I can't show everything I got from everyone so sorry if I didn't get it all in

I'm focusing on minimum bias results in this talk

Not every $R_{p\mathrm{Pb}}$ result takes the rapidity shift into account

I'm not going into any detail anywhere

Apologies in advance if I misrepresent anyone's results or fail to do them justice in such a talk

Why Study pA In the First Place?

- **Baseline Measurements (Control for AA)**
- **Interesting in and of Themselves**
- **Shadowing vs. Saturation**
- **Model Predictions**

d/$p+A$ As A Control Experiment

STAR away-side jets: d+Au like pp, not Au+Au, evidence for energy loss in the medium

Charmonium at the SPS: 'QGP' in S+U collisions vanishes when matter effects seen in pA included

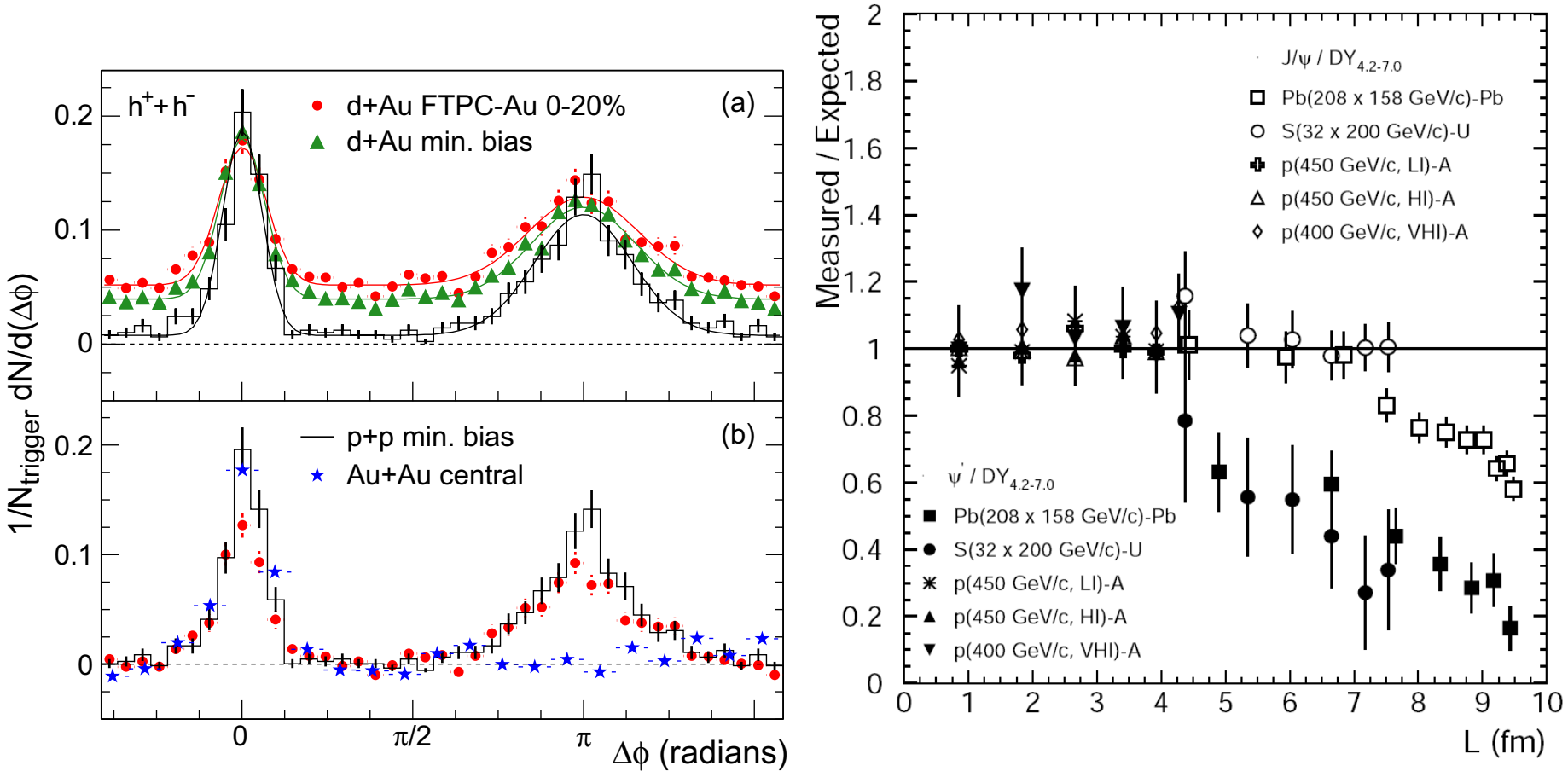

Figure 1: (Left) Comparison of azimuthal distributions in pp (solid histogram), d+Au (green triangles, min bias, and red circles, central) and Au+Au (blue stars) collisions at $\sqrt{s_{NN}} = 200$ GeV by STAR. [From STAR Collab., Phys. Rev. Lett. **91** (2003) 072304.] (Right) J/ψ and ψ' measurements at the CERN SPS, ratio of measured to expected in pA and AA systems.

Interesting in Their Own Right

Acoplanrity of Dijets in pA

Fermilab E609 pA at 400 GeV A = He, Be, C, Al, Cu, Sn, Pb measured $\Delta\phi$, azimuthal angle between jets, in pp and pA
Width of $\Delta\phi$ distributions used to obtain k_T, vector imbalance in p_T between jets

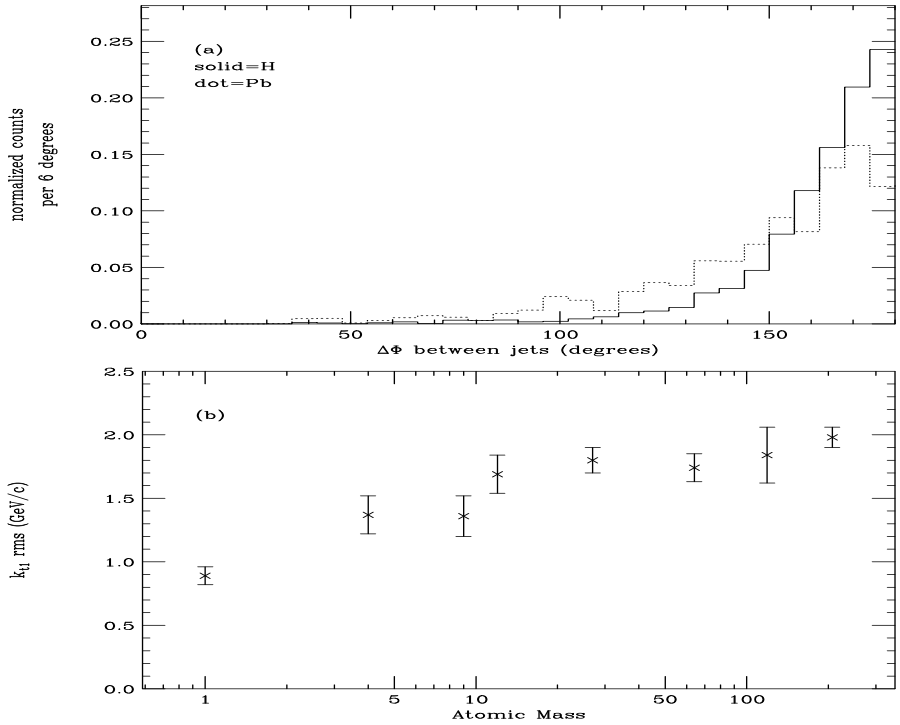

Figure 2: (a) The distribution in $\Delta\phi$. (b) The average value of k_{T1} as a function of A. The errors are statistical only. Required $p_T^{\rm jet} > 4$ GeV [From E609.]

A Dependence of J/ψ Stil Not Understood

Clear difference between J/ψ and ψ' effective absorption at midrapidity

Effective absorption cross section decreases with increasing $\sqrt{s}$

High x_F, forward rapidity data not well understood despite many attempts

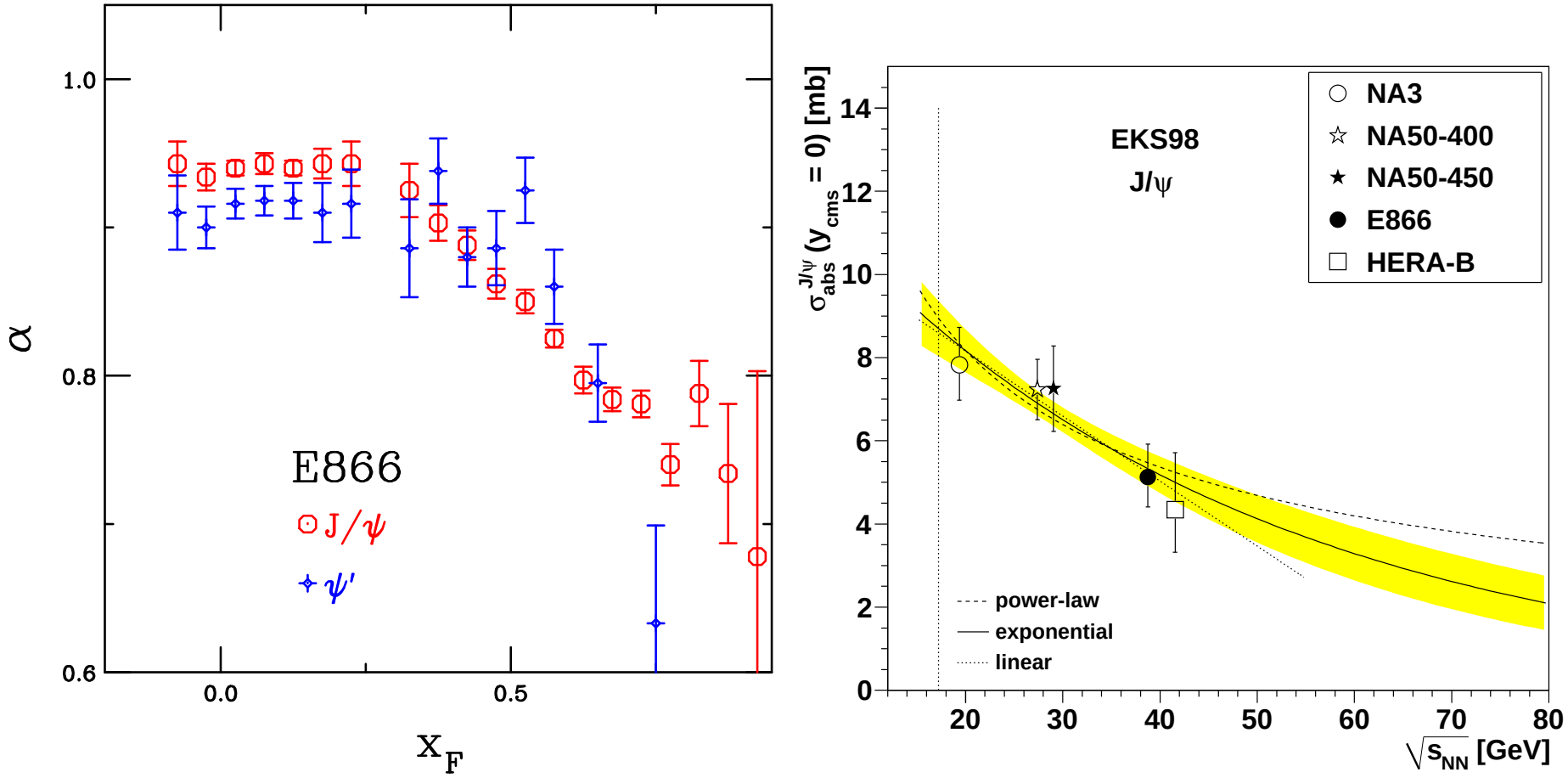

Figure 3: (Left) The J/ψ and ψ' A dependence as a function of x_F measured by the E866 Collaboration at $\sqrt{S_{NN}} = 38.8$ GeV. (Right) Energy dependence of absorption cross section extracted from $x_F \sim 0$ data by Lourenco, RV and Wöhri.

Parton Densities Modified in the Nucleus

Nuclear deep-inelastic scattering measures quark modifications directly

More uncertainty in nuclear gluon distribution, only indirectly constrained by Q^2 evolution of parton densities

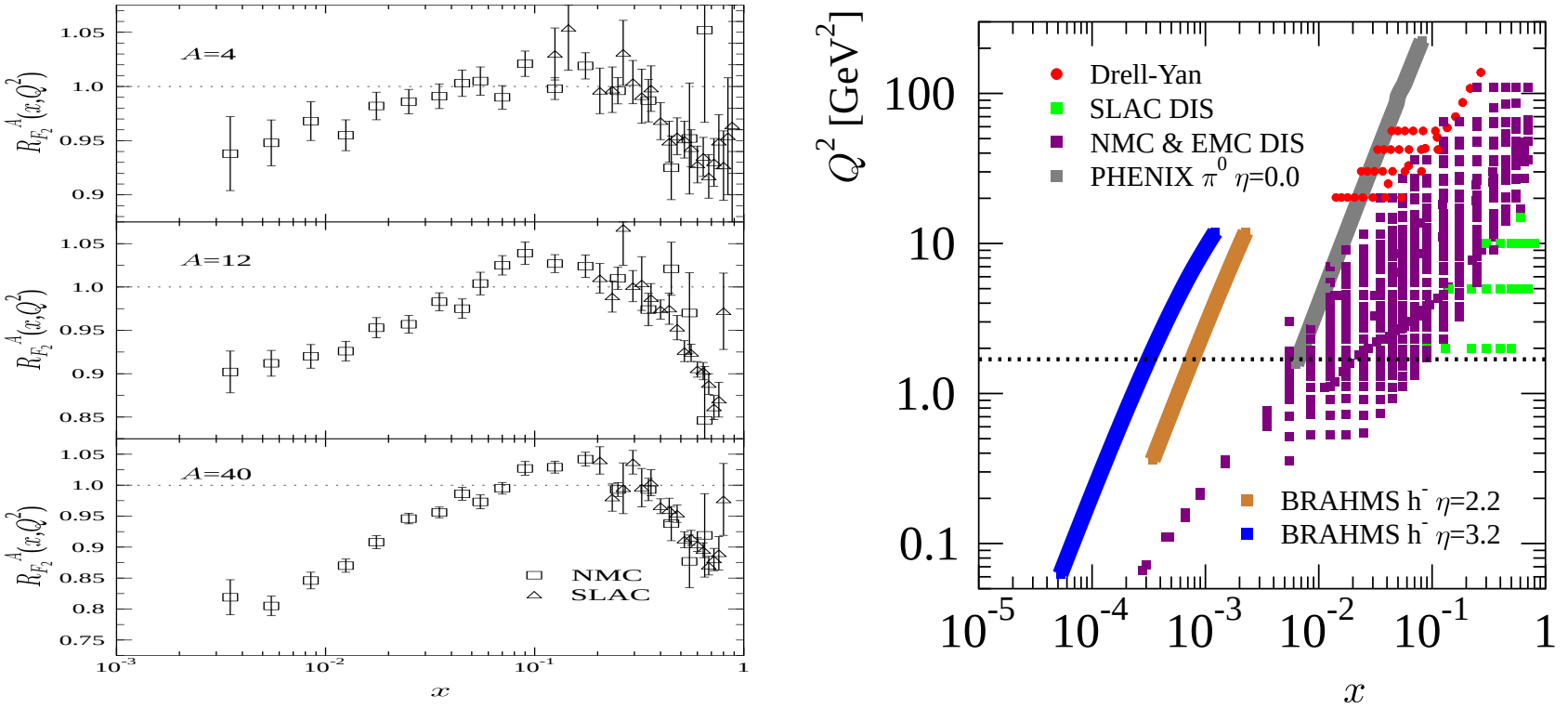

Figure 4: (Left) Ratios of charged parton densities in He, C, and Ca to D as a function of x. (Right) Evolution of gluon distributions in Sn relative to C targets with Q^2 for several fixed values of x.[From K.J. Eskola.]

x and Q^2 Reach of Heavy Ion Machines

p+Pb Collisions at the LHC are a factor of 25 higher energy than d+Au at RHIC, allowing broader range of cold matter studies in x and Q^2 than ever before

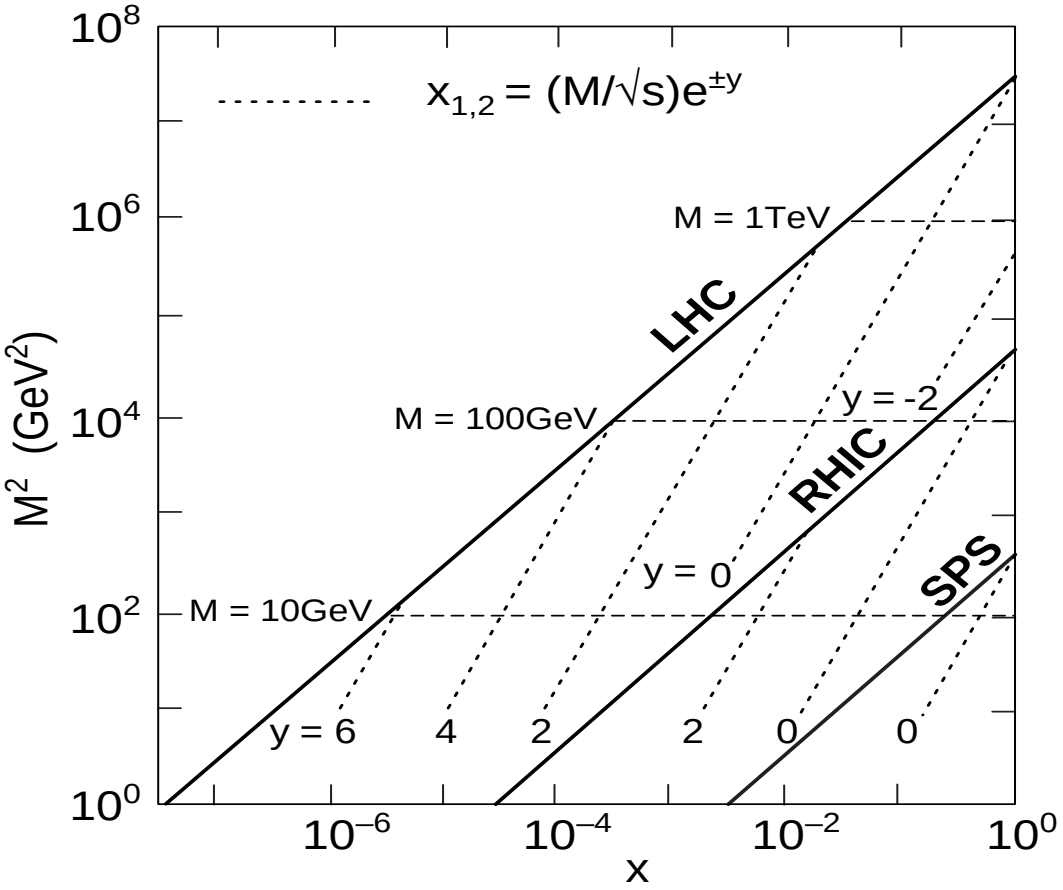

Figure 5: The Q^2 reach as a function of x for the SPS, RHIC and the LHC. Lines of constant rapidity are indicated for each machine.

Shadowing vs. Saturation

Shadowing
Starting with the Nucleus

Eskola *et al* Method I

Other groups use different data sets, initial assumptions, but similar methods – all start with nDIS data, usually with a minimum factorization/renormalization scale of $\sim 1-2$ GeV^2

Nuclear effects on PDFs divided into x regions

- **shadowing; a depletion at $x \lesssim 0.1$,**
- **anti-shadowing; an excess at $0.1 \lesssim x \lesssim 0.3$,**
- **EMC effect; a depletion at $0.3 \lesssim x \lesssim 0.7$**
- **Fermi motion; an excess towards $x \to 1$ and beyond.**

Define ratios of the individual and total valence and sea quark distributions and the gluon ratio in nuclei relative to protons

$$
\begin{aligned}
R^A_{\bar{q}}(x,Q^2) &\equiv \frac{\bar{q}_A(x,Q^2)}{\bar{q}(x,Q^2)} \quad R^A_{q_V}(x,Q^2) \equiv \frac{q^A_V(x,Q^2)}{q_V(x,Q^2)} \quad R^A_G(x,Q^2) \equiv \frac{g^A(x,Q^2)}{g(x,Q^2)} \\
R^A_V(x,Q^2) &\equiv \frac{u^A_V(x,Q^2)+d^A_V(x,Q^2)}{u_V(x,Q^2)+d_V(x,Q^2)}, \\
R^A_S(x,Q^2) &\equiv \frac{\bar{u}_A(x,Q^2)+\bar{d}_A(x,Q^2)+\bar{s}_A(x,Q^2)}{\bar{u}(x,Q^2)+\bar{d}(x,Q^2)+\bar{s}(x,Q^2)}
\end{aligned}
$$

Most groups now have NLO sets and some include uncertainties, *e.g.* EPS09 includes 31 sets: 1 central + 30 obtained by varying each parameter by one standard deviation

Eskola *et al* Method II

Determination of $R_i^A(x,Q^2)$ from nuclear deep-inelastic scattering (nDIS) and Drell-Yan (DY) data

- **Formulate $R_{F_2}^A(x,Q^2)$ and $R_{\rm DY}^A(x,Q^2)$ based on linear combinations of the quark and antiquark ratios**
- **Make an ansatz for $R_{F_2}^A(x,Q_0^2)$ based on nDIS data**
- **Decompose $R_{F_2}^A(x,Q_0^2)$ into R_V^A and R_S^A**
- **Constrain R_V^A using baryon number conservation**
  $\int_0^1 dx[u_V(x,Q_0^2)+d_V(x,Q_0^2)]R_V^A(x,Q_0^2) = \int_0^1 dx[u_V(x,Q_0^2)+d_V(x,Q_0^2)] = 3$
- **Constrain $R_G^A(x,Q_0^2)$ by momentum conservation (gluons removed at low x get put back at higher x, for stability of R_V^A and R_S^A assume gluon EMC effect)**
  $1 = \int_0^1 dx\, x\Big\{g(x,Q_0^2)R_G^A(x,Q_0^2)+[u_V(x,Q_0^2)+d_V(x,Q_0^2)]R_V^A(x,Q_0^2)+2[\bar{u}(x,Q_0^2)+\bar{d}(x,Q_0^2)+s(x,Q_0^2)]R_S^A(x,Q^2)\Big\}$
- **Perform DGLAP evolution of the initial nPDFs which can further constrain gluon shadowing**

$$\begin{aligned}\frac{\partial R_{F_2}^A(x,Q^2)}{\partial\log Q^2} &= \frac{\partial F_2^D(x,Q^2)/\partial\log Q^2}{F_2^D(x,Q^2)}\Big\{\frac{\partial F_2^A(x,Q^2)/\partial\log Q^2}{\partial F_2^D(x,Q^2)/\partial\log Q^2} - R_{F_2}^A(x,Q^2)\Big\}\\ &\approx \frac{5\alpha_s}{9\pi}\frac{xg(2x,Q^2)}{F_2^D(x,Q^2)}\Big\{R_G^A(2x,Q^2)-R_{F_2}^A(x,Q^2)\Big\}\end{aligned}$$

- **Constrain $R_S^A(x,Q_0^2)$ and $R_V^A(x,Q_0^2)$ with Drell-Yan data**
- **Repeat, repeat, repeat**

Comparison of LO and NLO nDS nPDFs

When data are available, LO and NLO shadowing results agree, as they are meant to

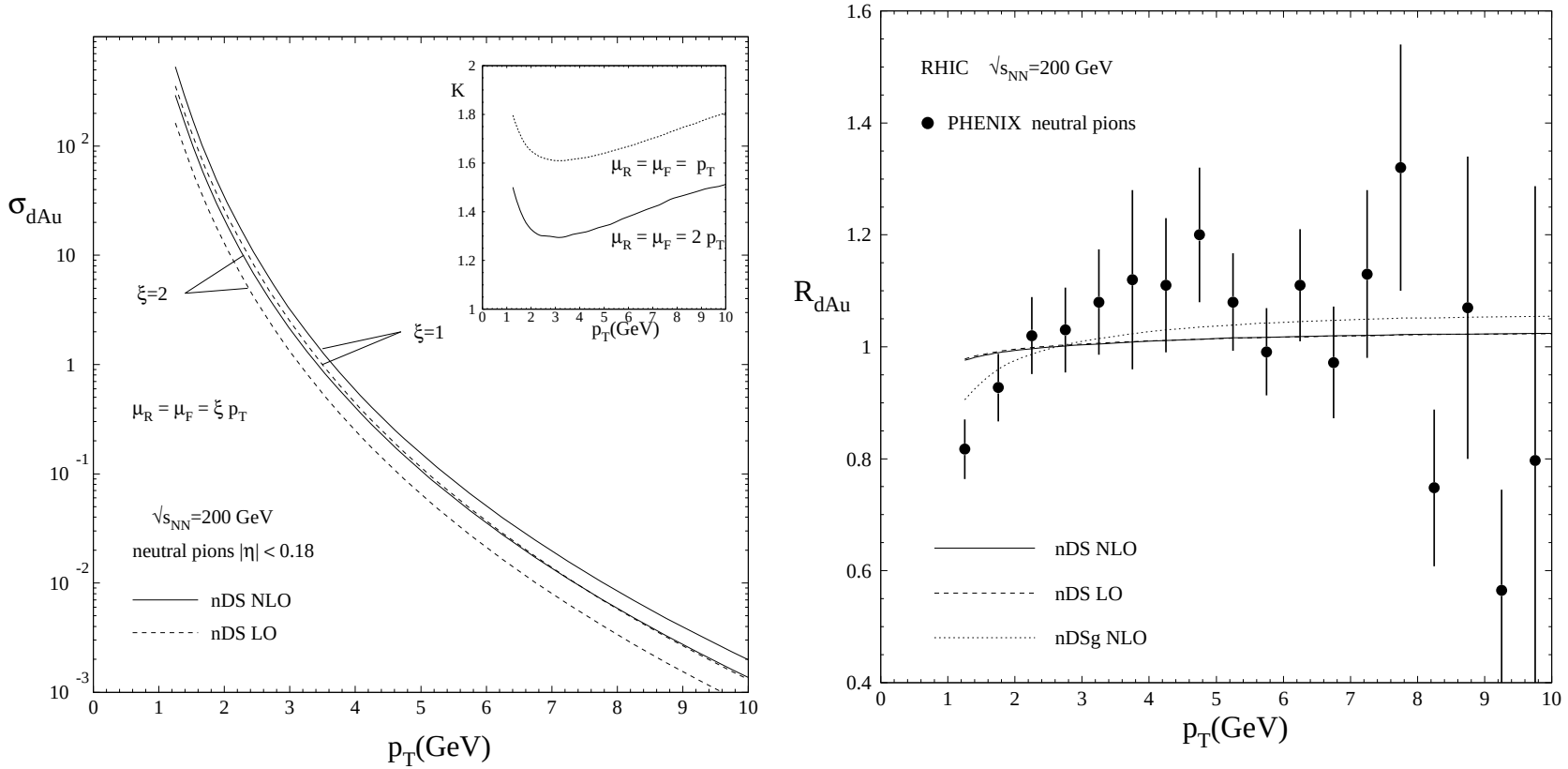

Figure 6: **(Left) The π^0 cross section in d+Au collisions at $\sqrt{s_{NN}} = 200$ GeV at LO and NLO. (Right) The LO and NLO calculations of $R_{\rm dAu}$, along with the NLO calculation with nDSg.**

Comparing Shadowing Parameterizations: x Dependence

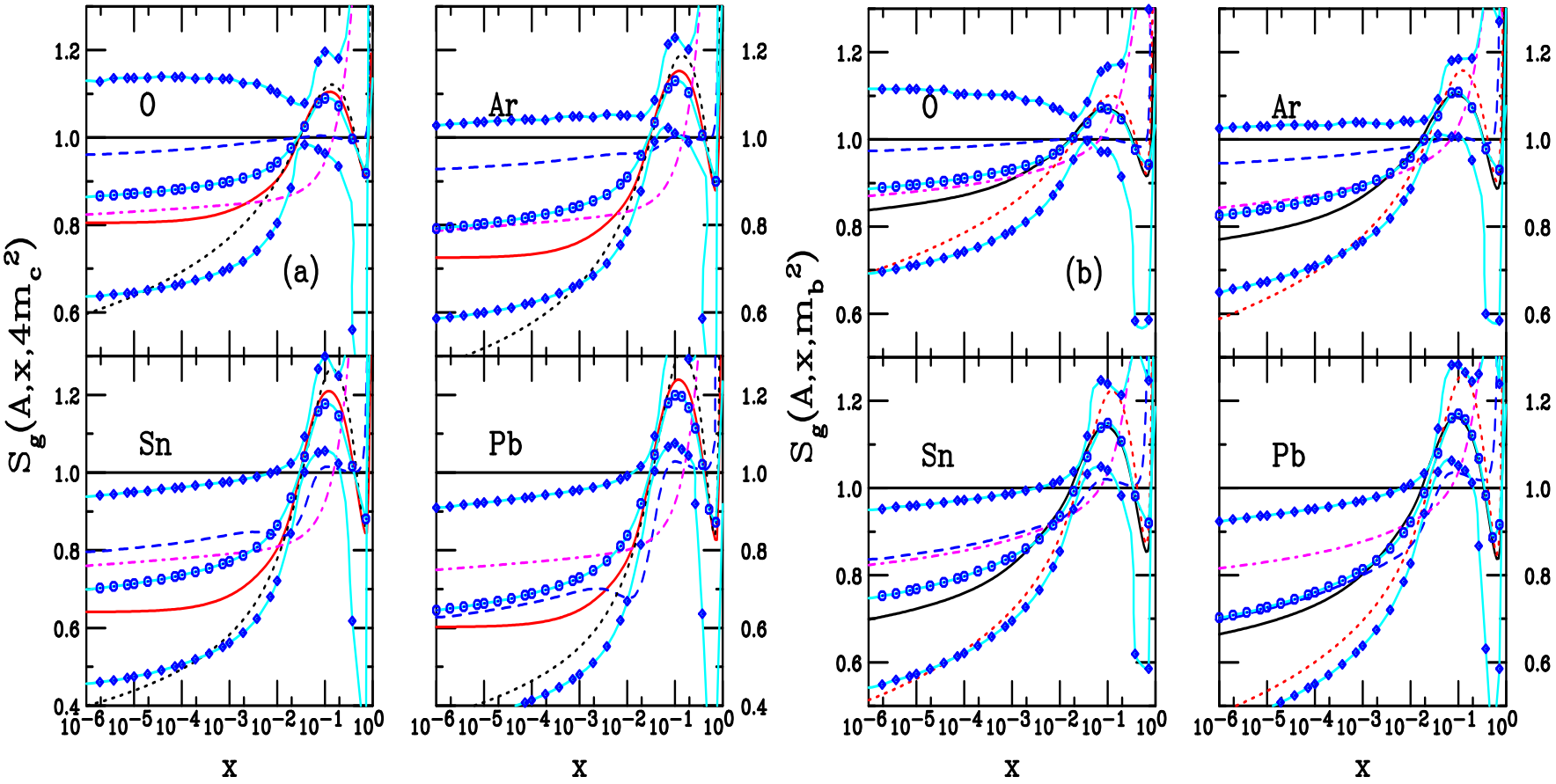

Figure 7: **Comparison of EKS98 (red), nDSg (blue), HKN (green), EPS08 (magenta), and EPS09 (cyan, with symbols) gluon shadowing parameterizations for J/ψ (left) and Υ (right) production scales with A =O, Ar, Sn and Pb.**

Saturation
Starting from the Nucleon (Naive picture)

Gluon Density in Hadrons

DGLAP QCD evolution predicts increase of parton densities at low x because DGLAP neglects interactions between partons, even at high parton density

At fixed Q^2 parton (gluon) distribution functions saturate at momentum scale $Q^2_{\rm sat}$,

$$Q^2_{\rm sat} = \alpha_s N_c \frac{1}{\pi R^2} \frac{dN}{dy}$$

Application makes sense when $Q^2_{\rm sat} \gg \Lambda^2_{\rm QCD}$ and $\alpha_s(Q^2_{\rm sat}) \ll 1$

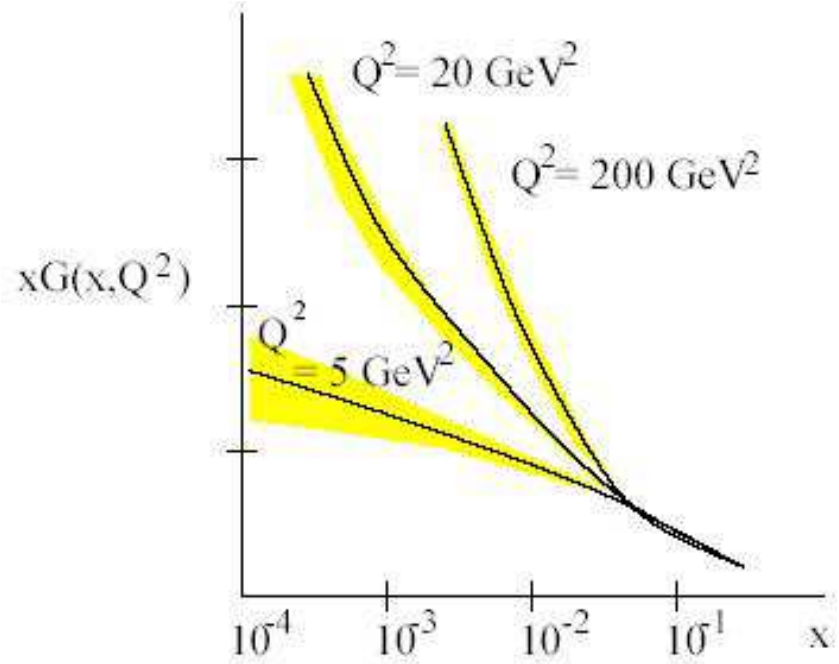

Figure 8: **Extraction of the gluon distribution in the proton by Zeus at $Q^2 = 5$, 20, and 200 GeV^2.**

F_2 Data Deviate from DGLAP at Low x and Q^2

At low x and moderate Q^2, the derivative of F_2 with respect to Q^2 is seen to deviate from PDF expectations

Caveat, comparison is to GRV94HO, a rather old set, may work to lower Q^2 with newer data

Differences appear at $x < 10^{-3}$ and $Q^2 < 9$ GeV^2

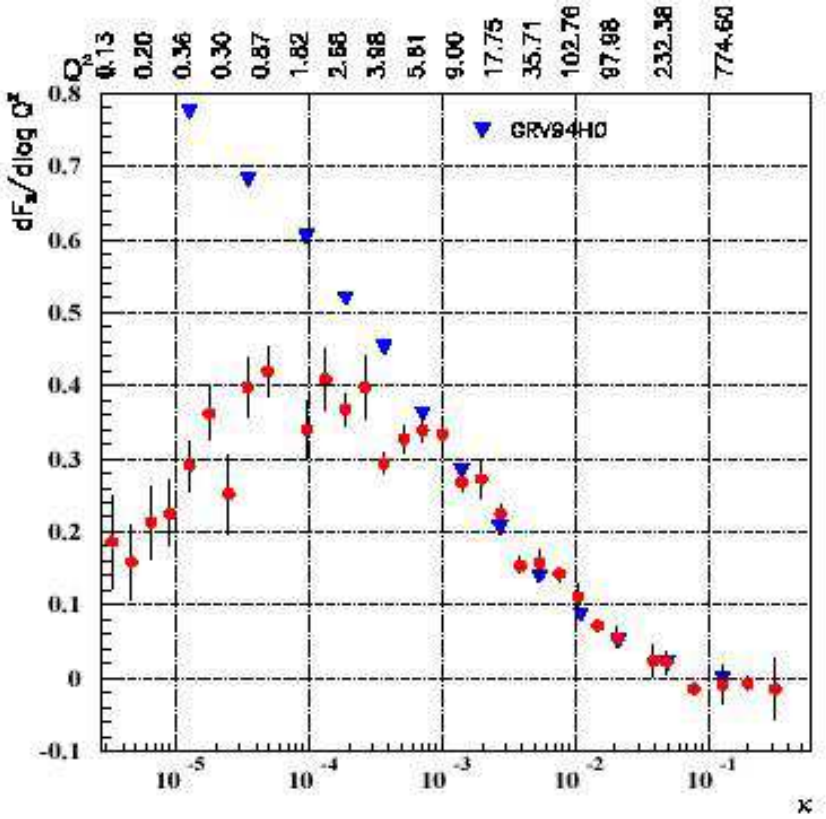

Figure 9: **The derivative $dF_2/d\ln Q^2$ as a function of x (bottom axis) and Q^2 (top axis). (From H. Abramowitz and A. Caldwell, DESY report 98-192 (1998))**

Schematic View of Saturation Regime

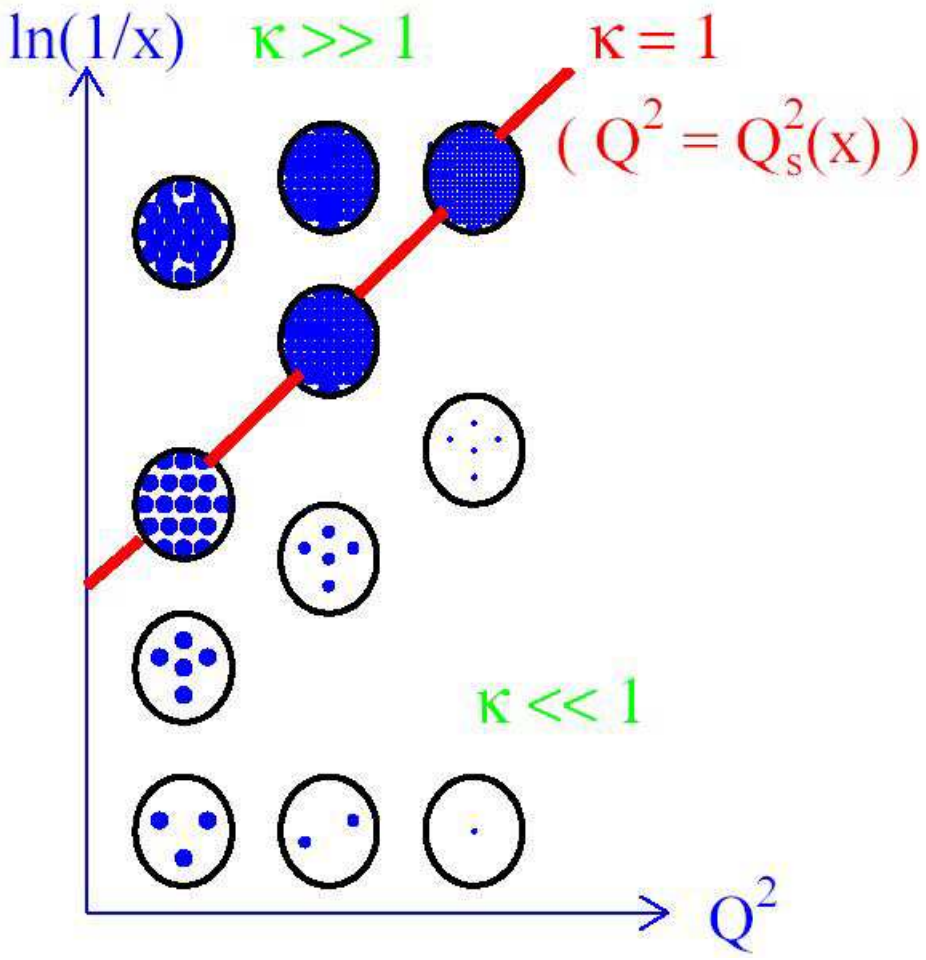

Saturation condition: when the gluon density, ρ_g, is sufficiently high, recombination of gluons $(2 \to 1)$ competes with emission of new partons $(1 \to 2)$ $\rho \sim 1/\alpha_s$

Packing factor: fraction of how much of nucleon/nuclear disk is packed with partons,
$\kappa = \sigma_{\rm dipole}/\pi R^2$, $\sigma_{\rm dipole} \propto F_2(x, Q^2)/Q^2$

$Q_{\rm sat}$ grows with increasing $\sqrt{s}$ and decreasing x

in nuclei $Q_{\rm sat}$ increases by $A^{1/3}$

Charged Particle Multiplicity and p_T Distributions

Results from the p+Pb Test Run

First ALICE $dN_{\rm ch}/d\eta$ data compared to models

Surprise: Saturation models don't do as well as may have been expected from RHIC

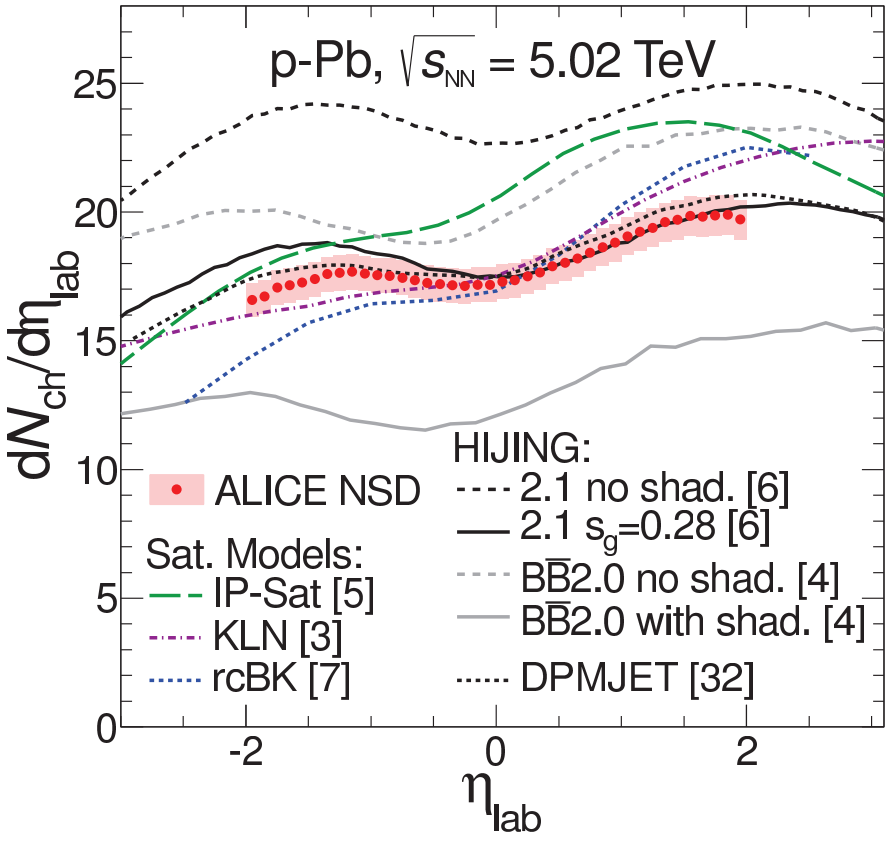

Figure 10: Charged particle psuedorapidity density measured in non-single diffractive p+Pb collisions at $\sqrt{s_{NN}} = 5.02$ TeV collisions compared to predictions. From ALICE Collaboration, arXiv:1210.3615 [nucl-ex].

Comparing the Lab to Center-of-Mass Frames

Most calculations done in CM Frame, shift to lab frame involves a shift of $\Delta y_{NN} = 0.465$ in the direction of the proton beam

Results in lab frame only shown for calculations when directly available from the source

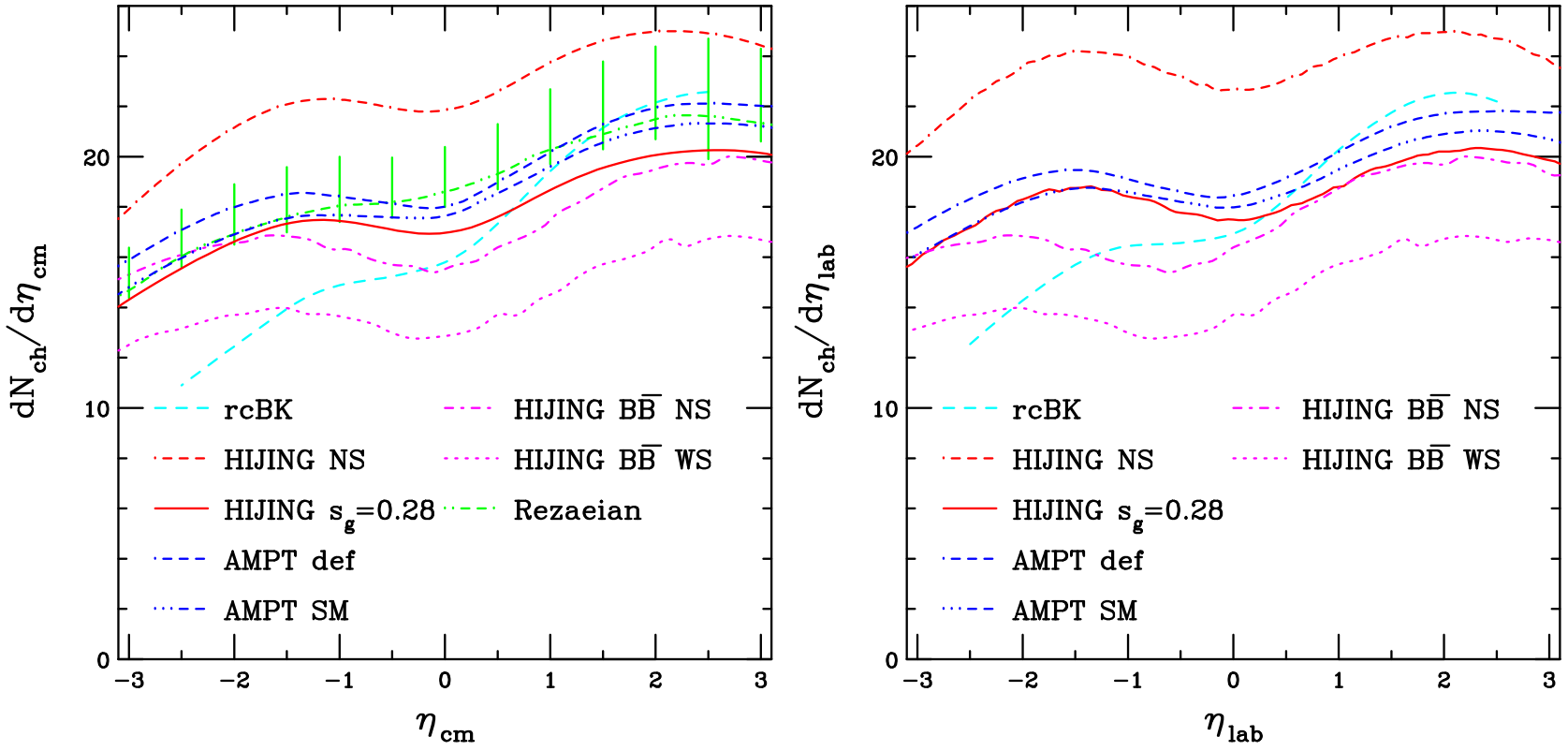

Figure 11: **Charged particle pseudorapidity distributions at $\sqrt{s_{NN}} = 5.02$ TeV in the CM (left) and lab (right) frames. Courtesy of Albacete *et al.*, XN Wang *et al.*, Z Lin, Rezaeian, and Topor Po *et al.*.**

Relative p and Pb Peak Ratios in Lab Frame

Models without saturation come closer to data as well as getting the forward/backward ratio right

	$dN_{\rm ch}/d\eta_{\rm lab}$			$R(\eta_{\rm lab}=2/\eta_{\rm lab}=-2)$
	-2	**0**	**2**	
ALICE	16.65 ± 0.65	17.24 ± 0.66	19.81 ± 0.78	1.19 ± 0.05
Saturation Models				
IP-Sat	**17.55**	**20.55**	**23.11**	**1.32**
KLN	**15.96**	**17.51**	**22.02**	**1.38**
rcBK	**14.27**	**16.94**	**22.51**	**1.58**
HIJING-based				
2.1 NS (no shad)	**23.58**	**22.67**	**24.96**	**1.06**
2.1 WS ($s_g = 0.28$)	**18.30**	**17.49**	**20.21**	**1.10**
B$\overline{\rm B}$ **NS***	**20.03**	**19.68**	**23.24**	**1.16**
B$\overline{\rm B}$ **NS**†	**16.84**	**16.39**	**19.68**	**1.16**
B$\overline{\rm B}$ **WS***	**12.97**	**12.09**	**15.16**	**1.17**
B$\overline{\rm B}$ **WS**†	**13.98**	**13.71**	**16.73**	**1.20**
AMPT				
Default	**19.07**	**18.56**	**21.65**	**1.14**
String Melting	**18.14**	**18.10**	**20.84**	**1.15**
DPMJET	**17.50**	**17.61**	**20.67**	**1.18**

Table 1: **Comparison of values of $dN_{\rm ch}/d\eta_{\rm lab}$ at $\eta_{\rm lab} = -2$, 0, 2 and the ratio $dN_{\rm ch}/d\eta_{\rm lab}|_{\eta_{\rm lab=2}}/dN_{\rm ch}/d\eta_{\rm lab}|_{\eta_{\rm lab=-2}}$, denoted by R above. The $*$ on HIJING B$\overline{\rm B}$ indicates that the calculations have been shifted to the lab frame by the ALICE Collaboration while the † are results provided by V. Topor Pop. Adapted from ALICE Collaboration, arXiv:1210.3615 [nucl-ex].**

Charged Particle p_T Distributions

Results similar at low p_T but deviate significantly at higher p_T
rcBK distributions do not differ strongly between $\eta = 0$ and 2

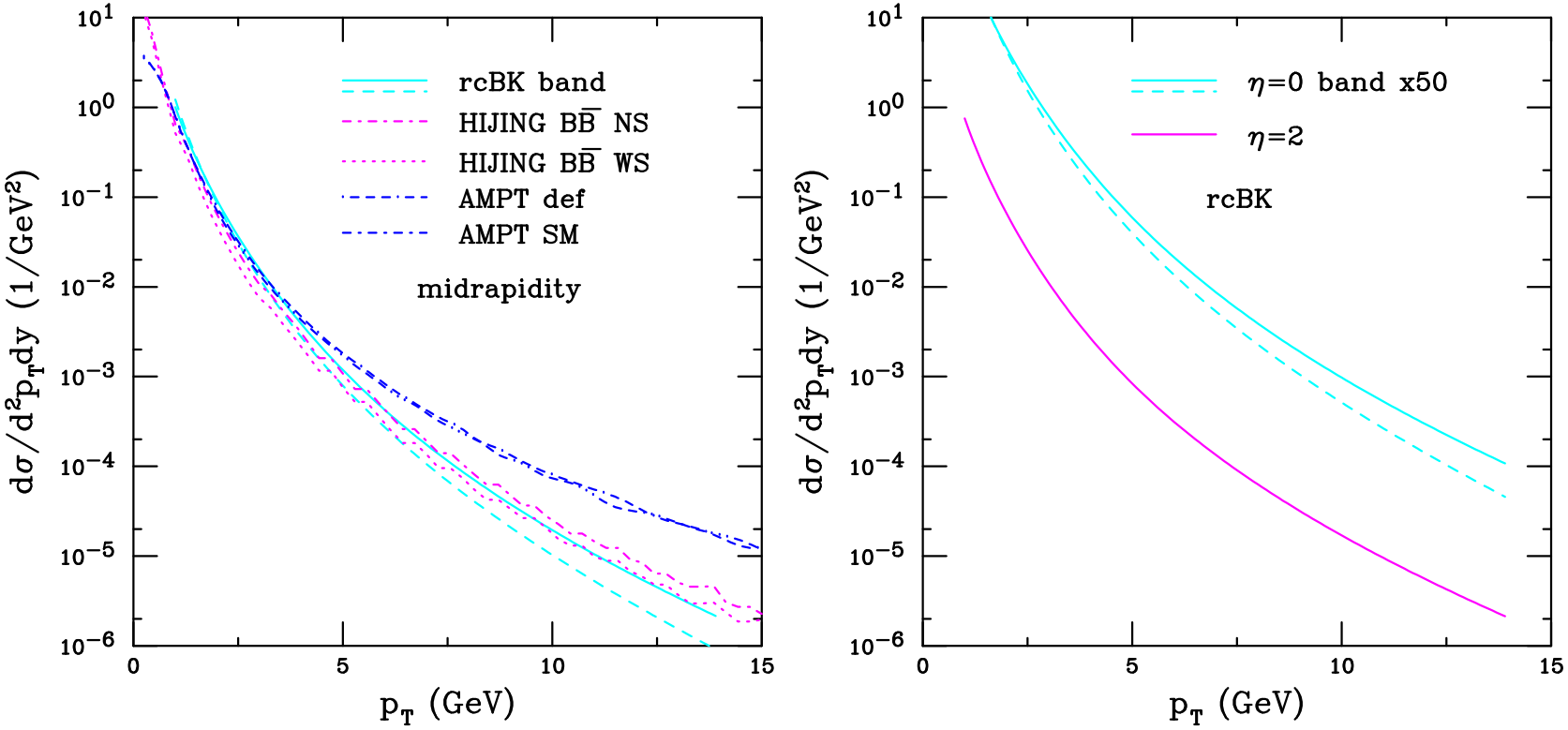

Figure 12: **Charged particle p_T distributions at $\sqrt{s_{NN}} = 5.02$ TeV at $\eta \sim 0$ (left) and comparing $\eta = 0$ and 2 in the rcBK saturation model (right). Courtesy of Albacete *et al.*, Topor Pop *et al.*, and Z. Lin.**

Caveat on Ratios

We already saw the difference in $dN_{\rm ch}/d\eta$ for p+Pb in the center of mass and the lab frames because $\Delta y_{_{NN}} = 0.465$

The pp η distribution is still symmetric around $\eta = 0$, no difference between center of mass and lab frames

Ratios are calculated without taking $\Delta y_{_{NN}}$ into account

It would be nice to have the pp data at $\sqrt{s_{_{NN}}} = 5.02$ TeV as well for more direct comparisons

Results from the p+Pb Test Run

ALICE $R_{p\mathrm{Pb}}$ data uses pp reference obtained by interpolating between data at 2.76 and 7 TeV, R_{pA} is formed by comparing $|\eta_{\mathrm{lab}}| < 0.8$ in p+Pb to $-0.3 < \eta_{\mathrm{cm}} < 1.3$; calculation of $\eta_{\mathrm{cm}} = \eta_{\mathrm{lab}} + 0.465$ is accurate for $m \sim 0$ or high p_T

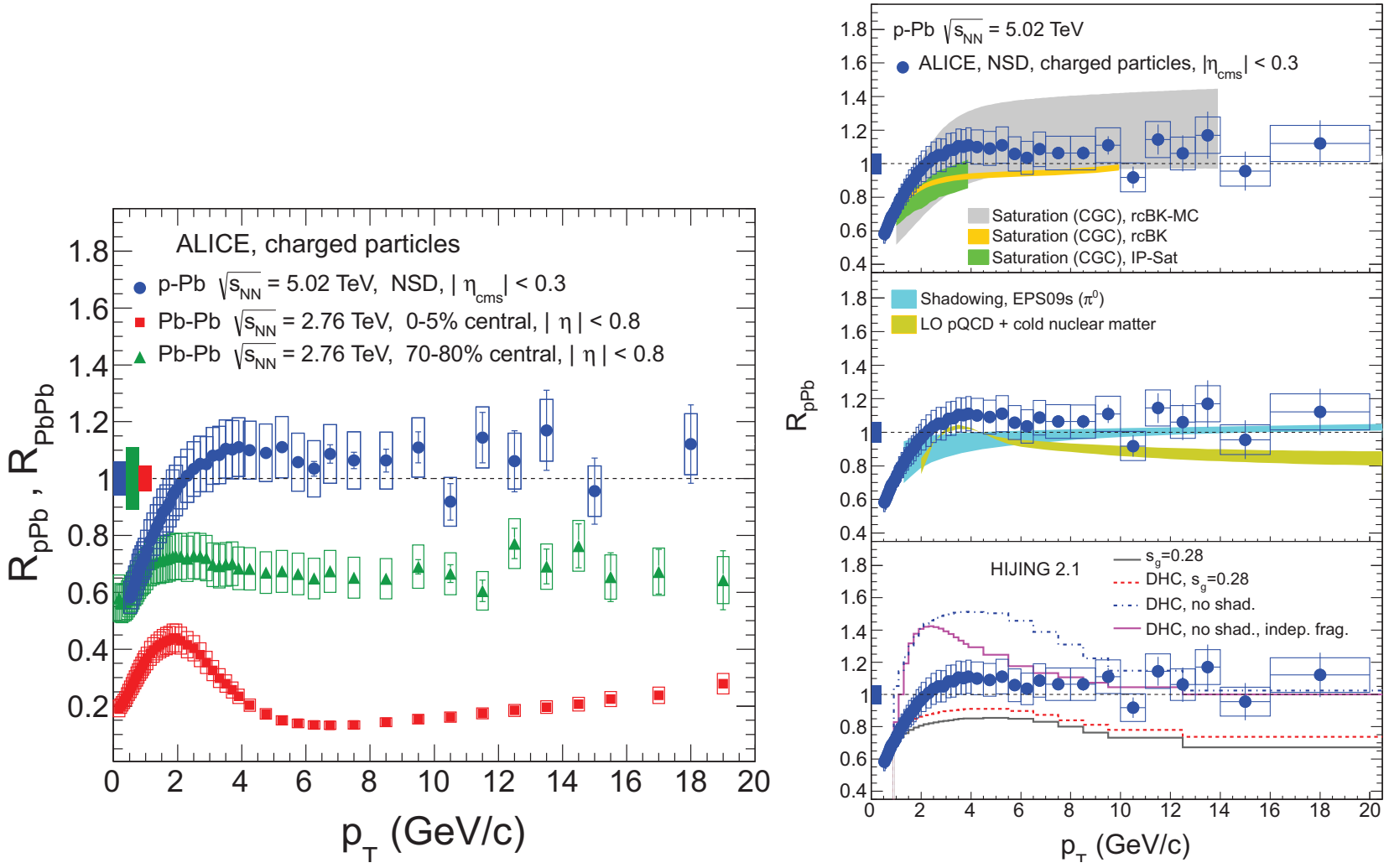

Figure 13: The minimum bias $R_{p\mathrm{Pb}}$ ratio is compared to central and peripheral values of R_{AA} (left) and various models (right). From ALICE Collaboration, arXiv:1210.4520 [nucl-ex].

$R_{p\mathrm{Pb}}$ for Charged Particles at Midrapidity

Wide range of predictions: standard shadowing parameterizations predict small effect with little p_T dependence

Some generators show large differences in $R_{p\mathrm{Pb}}$ due to shadowing but others do not

Large bands for saturation predictions (rcBK and Rezaeian)

Vitev result includes Cronin effect, cold matter energy loss, and shadowing, difference is whether parameters change with $\sqrt{s}$ or not

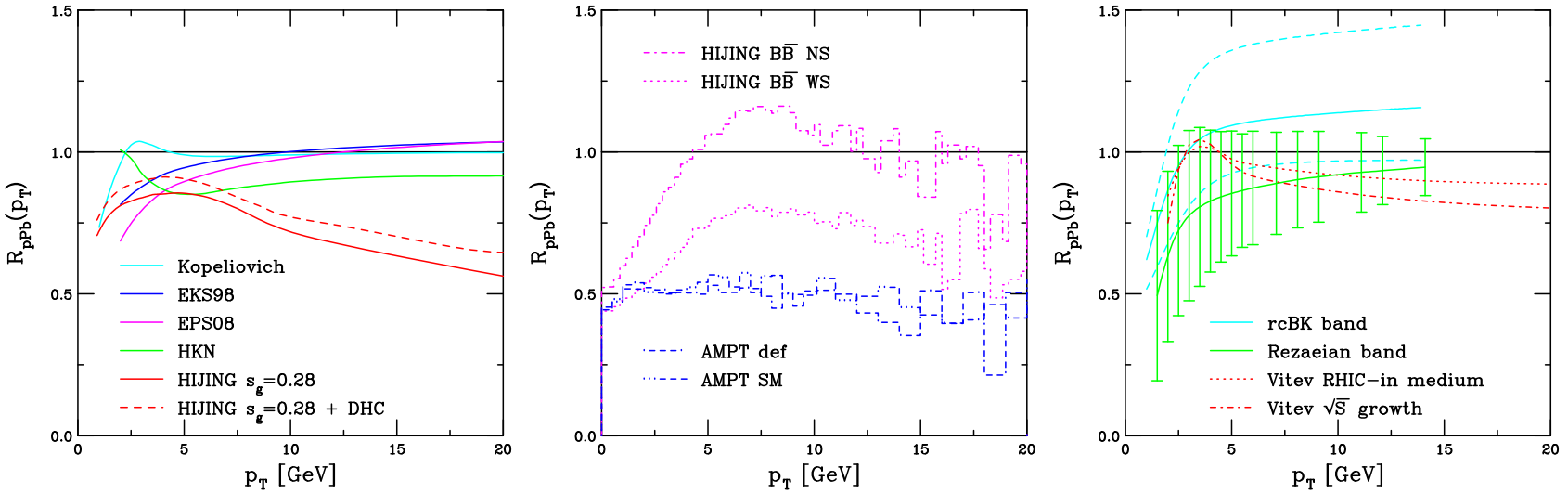

Figure 14: **Charged particle $R_{p\mathrm{Pb}}p_T$ at $\sqrt{s_{NN}} = 5.02$ TeV at $\eta \sim 0$. (Left) Results with more 'standard' shadowing (Barnafoldi *et al.* are compared. The difference in the HIJING curves depends on whether the hard scatterings are coherent or not. (Center) HIJING $\mathrm{B\overline{B}}$ (Topor Pop *et al.*) with and without shadowing compared to AMPT (Z. Lin) default and with string melting. (Right) The band from saturation models by Albacete *et al.* (rcBK) and Rezaeian are compared to a calculation by Vitev and collaborators.**

Identified Particles

$R_{p\mathrm{Pb}}$ for Neutral Pions

EPS09 shadowing + isospin gives enhancement at $y = 0$, including Cronin and energy loss results in reduction

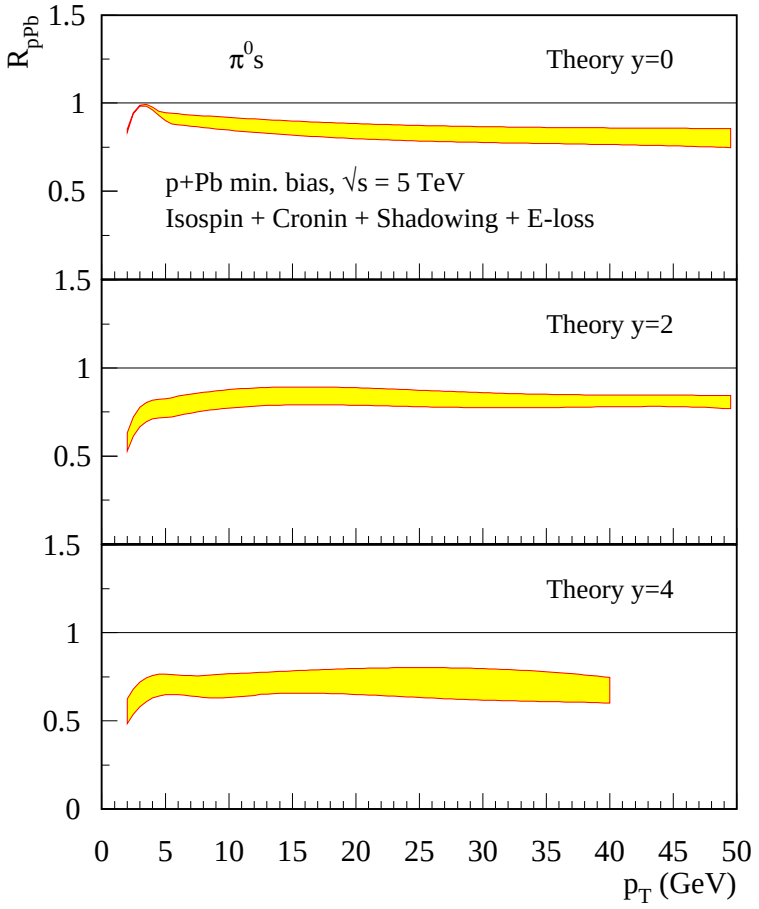

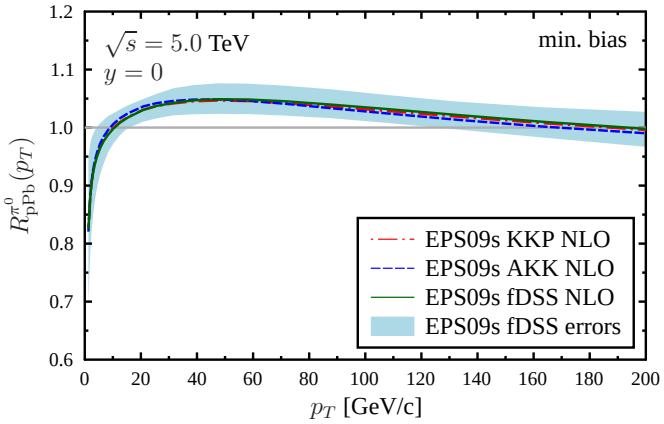

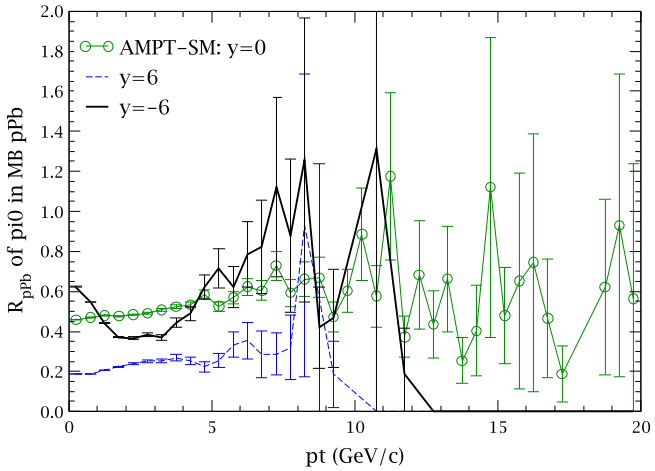

Figure 15: (Left) Vitev *et al.* predictions at $y = 0$, 2 and 4. (Upper Right) Eskola *et al.* comparing different fragmentation functions as well as delineating the EPS09s uncertainties. (Lower Right) AMPT predictions for several rapidities. Courtesy of I. Vitev, Eskola *et al.*, and Z. Lin.

AMPT Ratios for p vs. $\overline{p}$

Definite differences between proton and antiproton ratios, especially at negative rapidities

Statistical uncertainites large, especially at $p_T > 5$ GeV

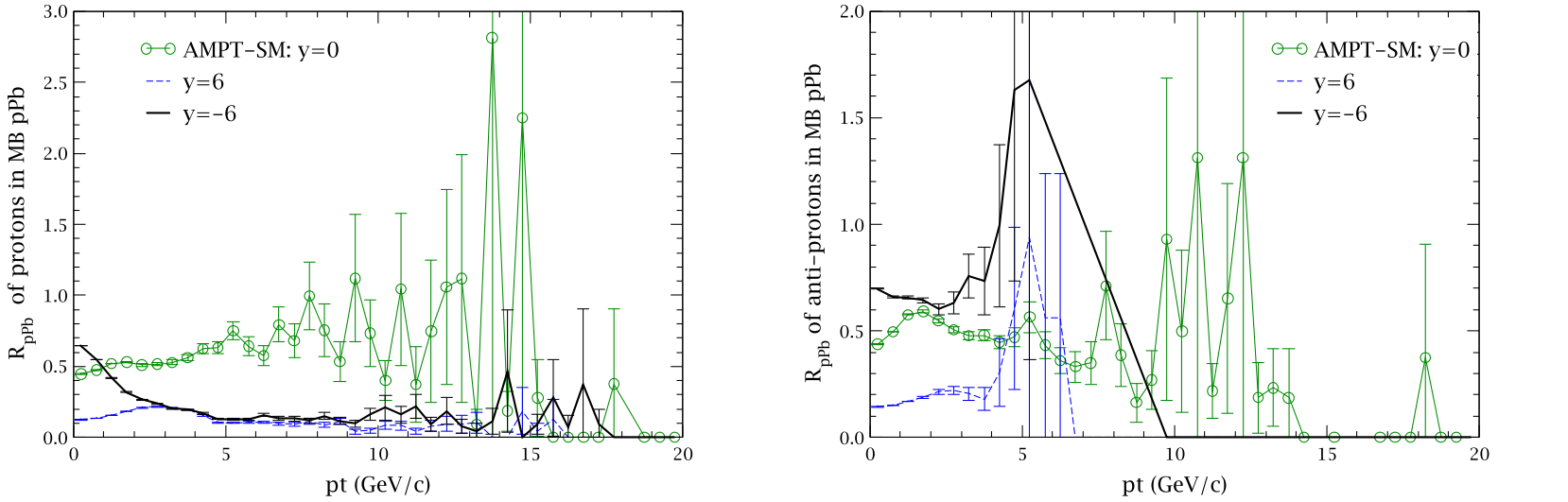

Figure 16: **The ratio $R_{p\mathrm{Pb}}(p_T)$ calculated with AMPT including string melting at $y = -6$, 0, and 6 for protons (left) and antiprotons (right). Courtesy of Z. Lin.**

Jets

Multiple Jet Production in Different Rapidity Intervals

NLO jet cross sections and yields for one, two and three jets

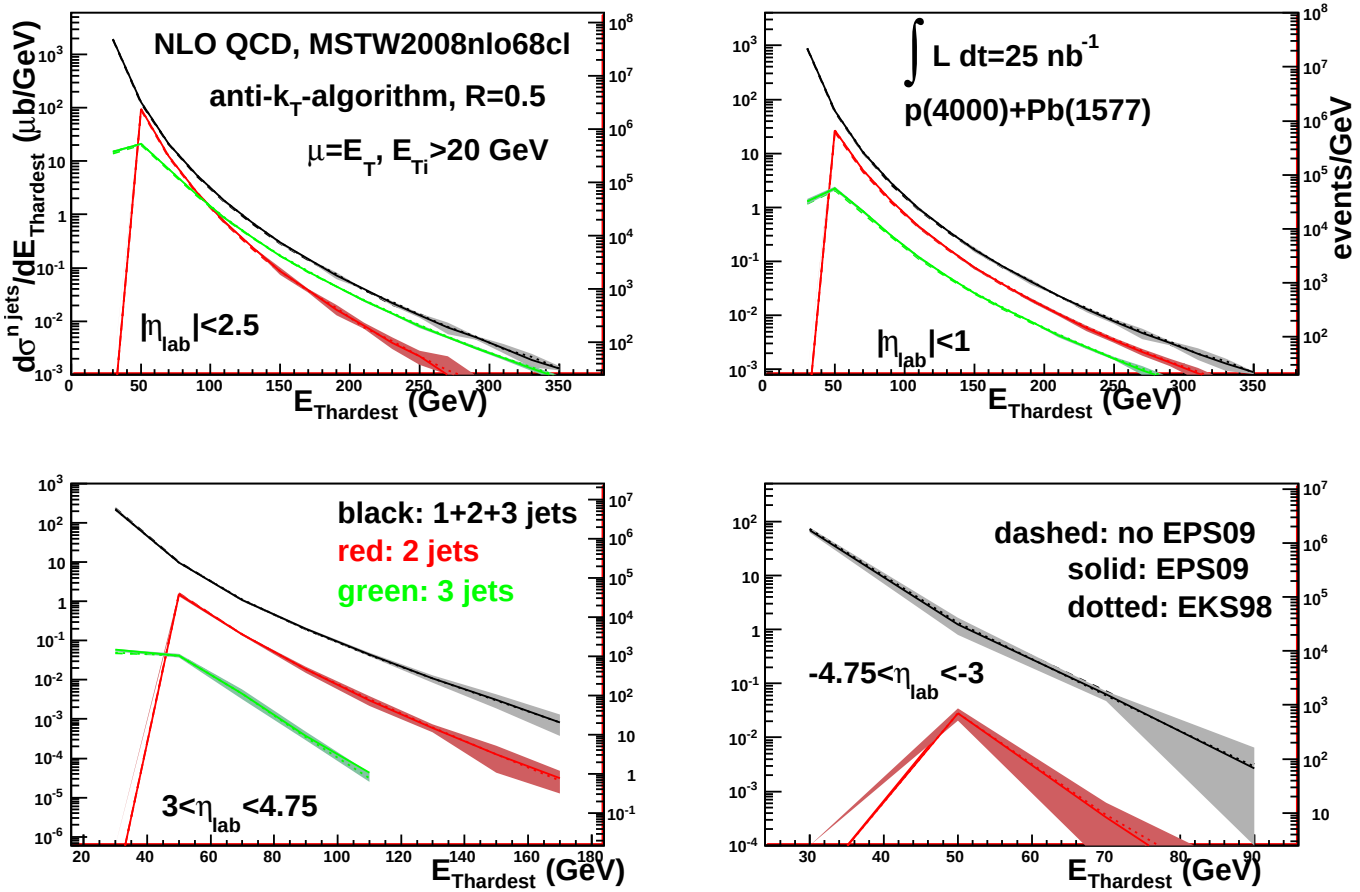

Figure 17: **Sum of the one, two and three jets (black), two jets (red) and three jets (green) cross sections as a function of the E_T of the hardest jet within the acceptance. Different pseudorapidity windows (in the lab frame) computed for minimum bias p+Pb collisions at the LHC (4+1.58 TeV per nucleon) are considered. Dashed lines are the results without nuclear modification to the PDFs; solid lines are the results with EPS09NLO; dotted lines are results with EKS98. The bands correspond to the EPS09 uncertainties. The right-hand y-axes give the corresponding yields for an integrated luminosity of 25 nb^{-1}. Courtesy of Nestor Armesto.**

Cold Matter Effects on Single and Dijet Production

Jet $R_{p\mathrm{Pb}}$ small, not a strong function of E_T

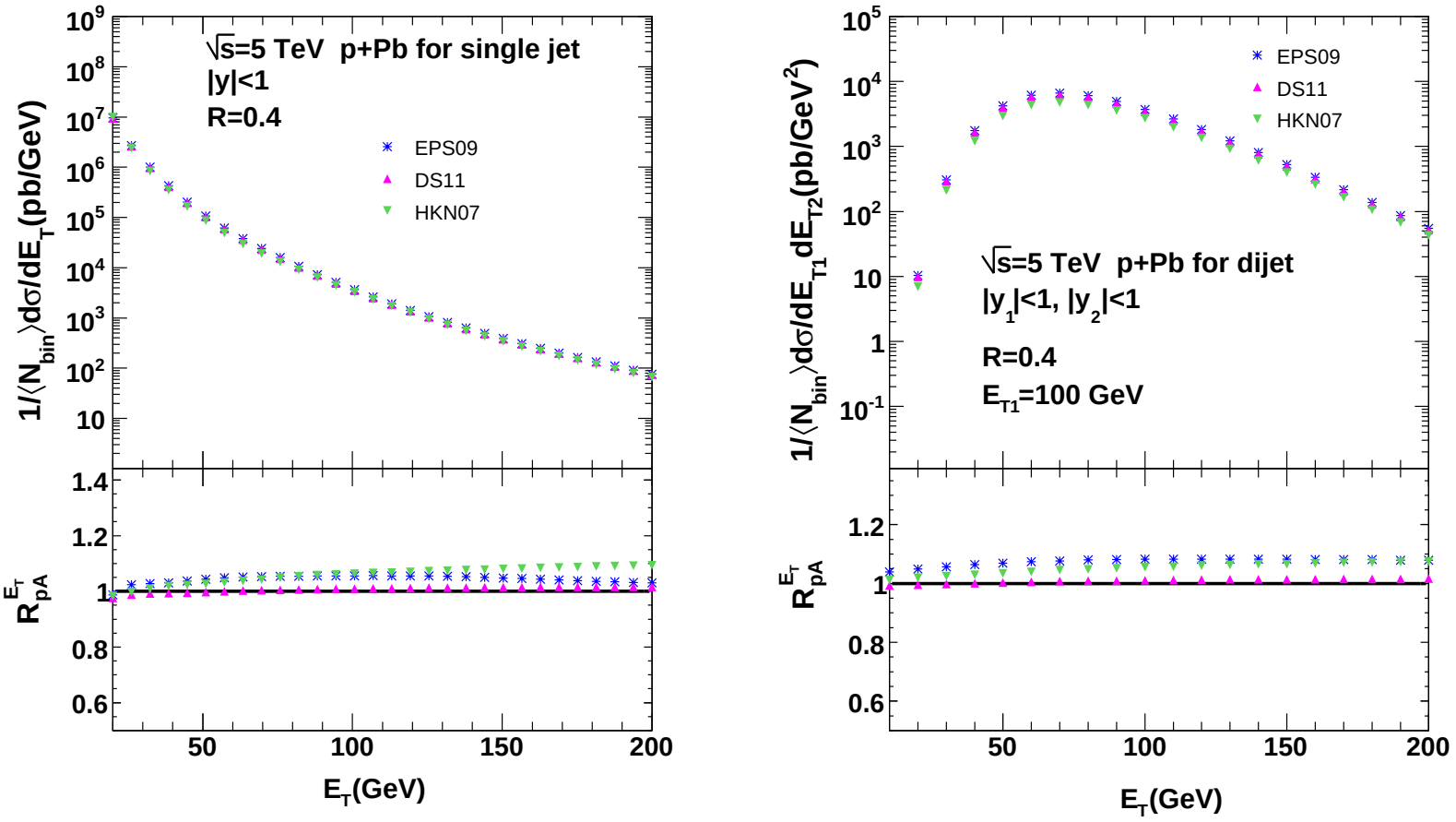

Figure 18: The inclusive jet spectra (left) and dijet E_T spectra with fixed energy $E_{T1} = 100$ GeV (right) in p+Pb collisions at $\sqrt{s} = 5$ TeV and the nuclear modification factors with three sets of nPDFs. Courtesy of Zhang *et al.*.

Medium Modifications of Jets

Left: Change in azimuthal distance between jets in saturated medium
Right: Estimate of jet broadening in medium

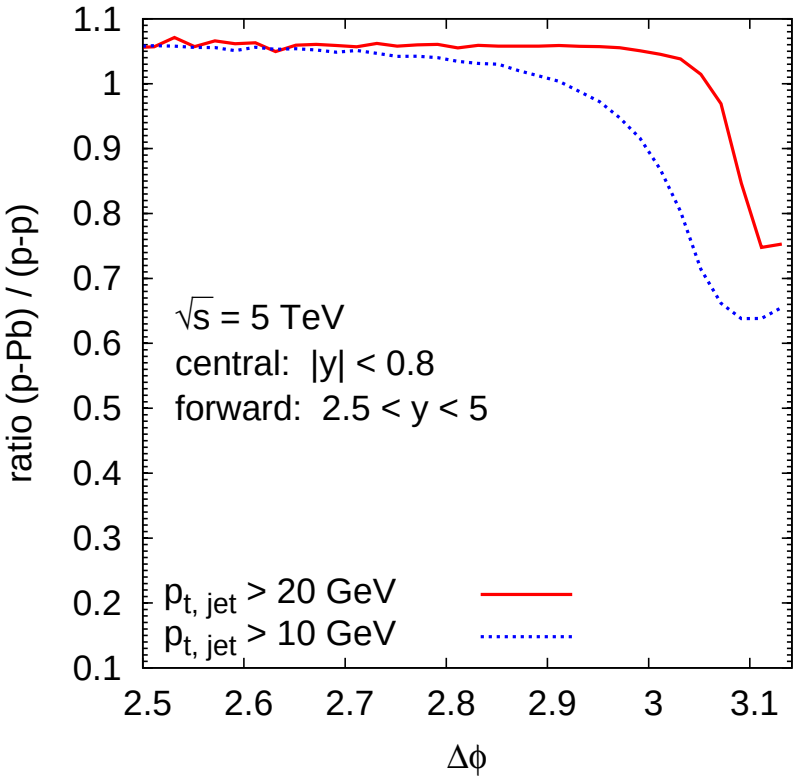

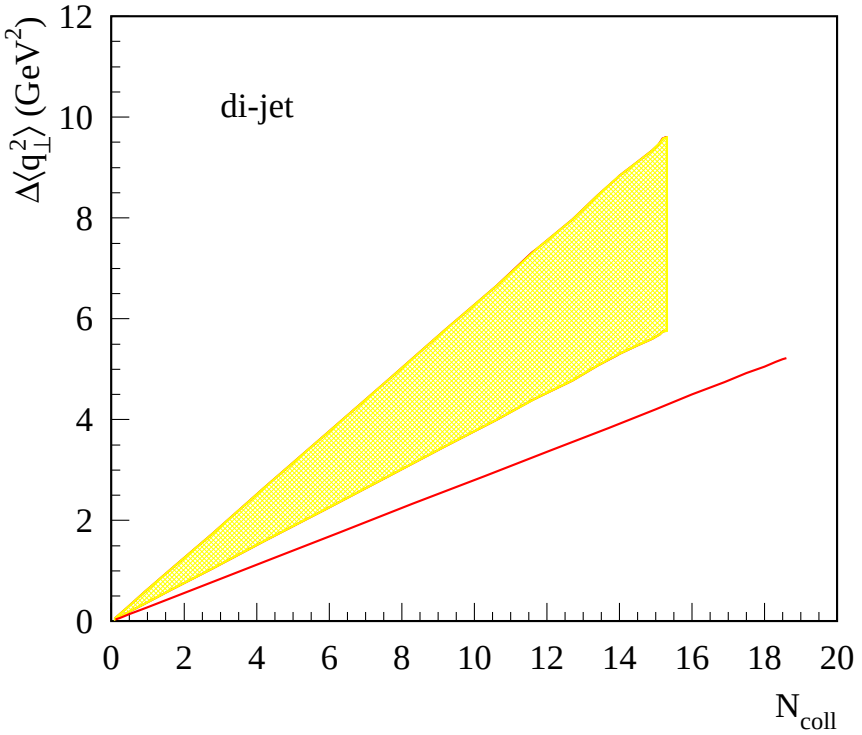

Figure 19: (Left) Ratio of differential cross sections for central and forward dijet production at $\sqrt{s} = 5$ TeV as a function of the azimuthal distance between the jets, $\Delta\phi$, for pp and p+Pb collisions with two different cuts on the jets p_T. Courtesy of Kryzstof Kutak. (Right) Nuclear broadening $\Delta\langle q_\perp^2 \rangle$ for dijets in pA collisions as a function of $N_{\rm coll}$. The fixed rapidities $y_1 = y_2 = 2$ are used for $\sqrt{s} = 5$ TeV LHC p+Pb collisions while $y_1 = y_2 = 1$ is used for the $\sqrt{s} = 200$ GeV RHIC d+Au collisions. For the LHC, the jet transverse momentum is integrated over $30 < p_T << 40$ GeV, while for RHIC the jet transverse momentum is integrated over $15 < p_T < 25$ GeV. The yellow band is for LHC kinematics, with the band representing a variation of the scattering parameter ξ^2. The red solid curve is for RHIC kinematics. Courtesy of Ivan Vitev.

Photons

Direct Photon Production in pQCD

Direct photon spectra for pp compared to p+Pb

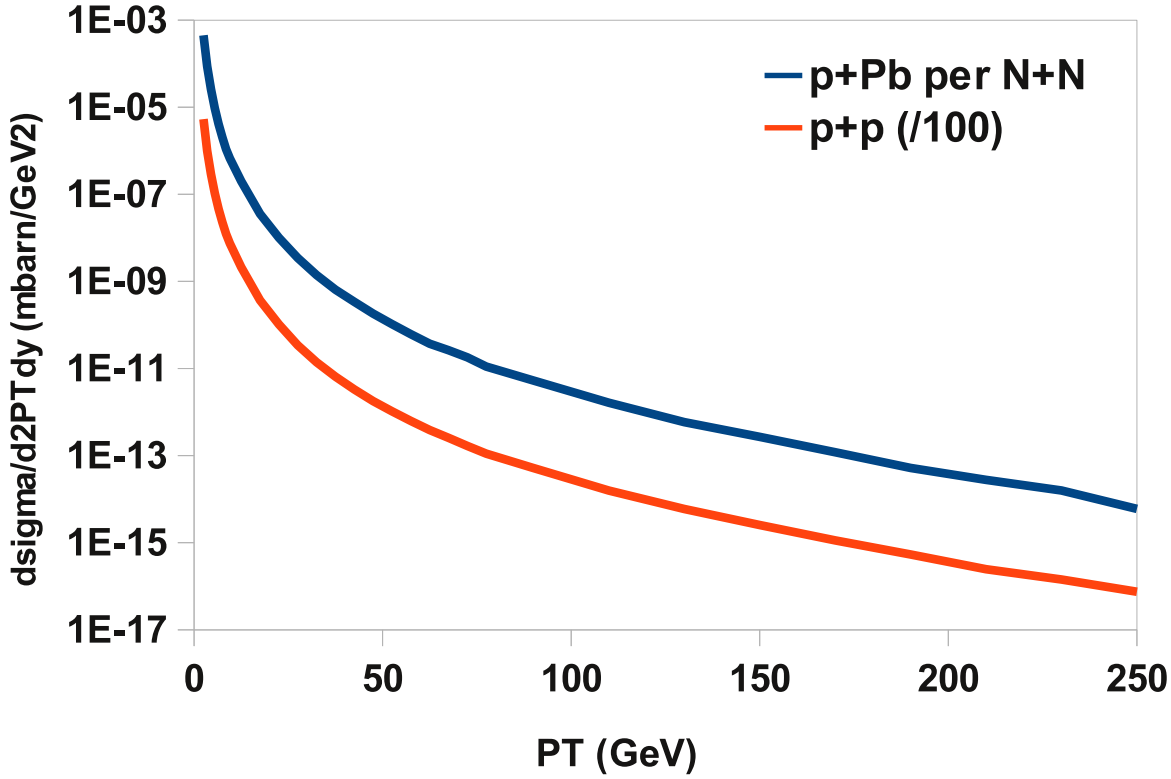

Figure 20: **The spectrum of direct photons $d\sigma/d^2P_T dy$ at in mb/GeV^2 for pp and p+Pb collisions at $\sqrt{s_{NN}} = 5$ TeV. The p+Pb cross section is normalized to one proton-nucleon collision. An isolation cut of $E_T < 5$ GeV for hadronic energy within a $R = 0.4$ cone has been imposed. The spectrum is shown for the center of mass frame of the collisions. In particular, in the lab frame the spectrum is for $y_{\rm lab} = 0$ for pp and $y = 0.47$ (in the direction of the proton) for p+Pb. The calculations were performed employing jetphox (Catani *et al.*) with EPS09 for the parton densities. Courtesy of R. Fries.**

Medium Modifications with Photon Production

Left: Results at different rapidities.

Right: Estimate of photon+jet broadening in medium

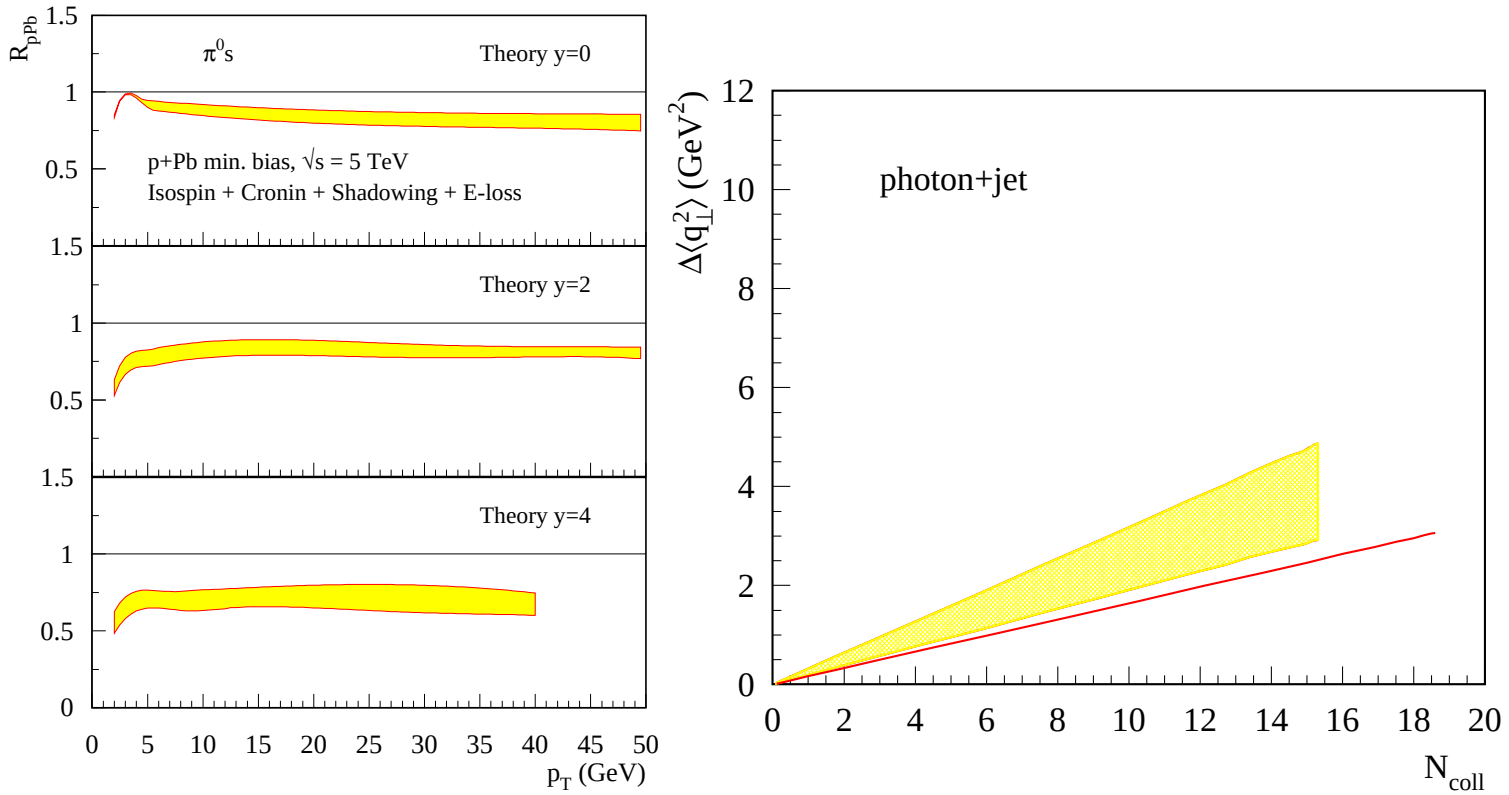

Figure 21: (Left) Vitev *et al.* predictions of photon+jet production at $y = 0$, 2 and 4. (Right) Nuclear broadening $\Delta\langle q_\perp^2\rangle$ for photon+jet production in pA collisions as a function of $N_{\rm coll}$. The fixed rapidities $y_1 = y_2 = 2$ are used for $\sqrt{s} = 5$ TeV LHC p+Pb collisions while $y_1 = y_2 = 1$ is used for the $\sqrt{s} = 200$ GeV RHIC d+Au collisions. For the LHC, the jet transverse momentum is integrated over $30 < p_T << 40$ GeV, while for RHIC the jet transverse momentum is integrated over $15 < p_T < 25$ GeV. The yellow band is for LHC kinematics, with the band representing a variation of the scattering parameter ξ^2. The red solid curve is for RHIC kinematics. Courtesy of Ivan Vitev.

J/ψ

nPDF Effects on J/ψ Production

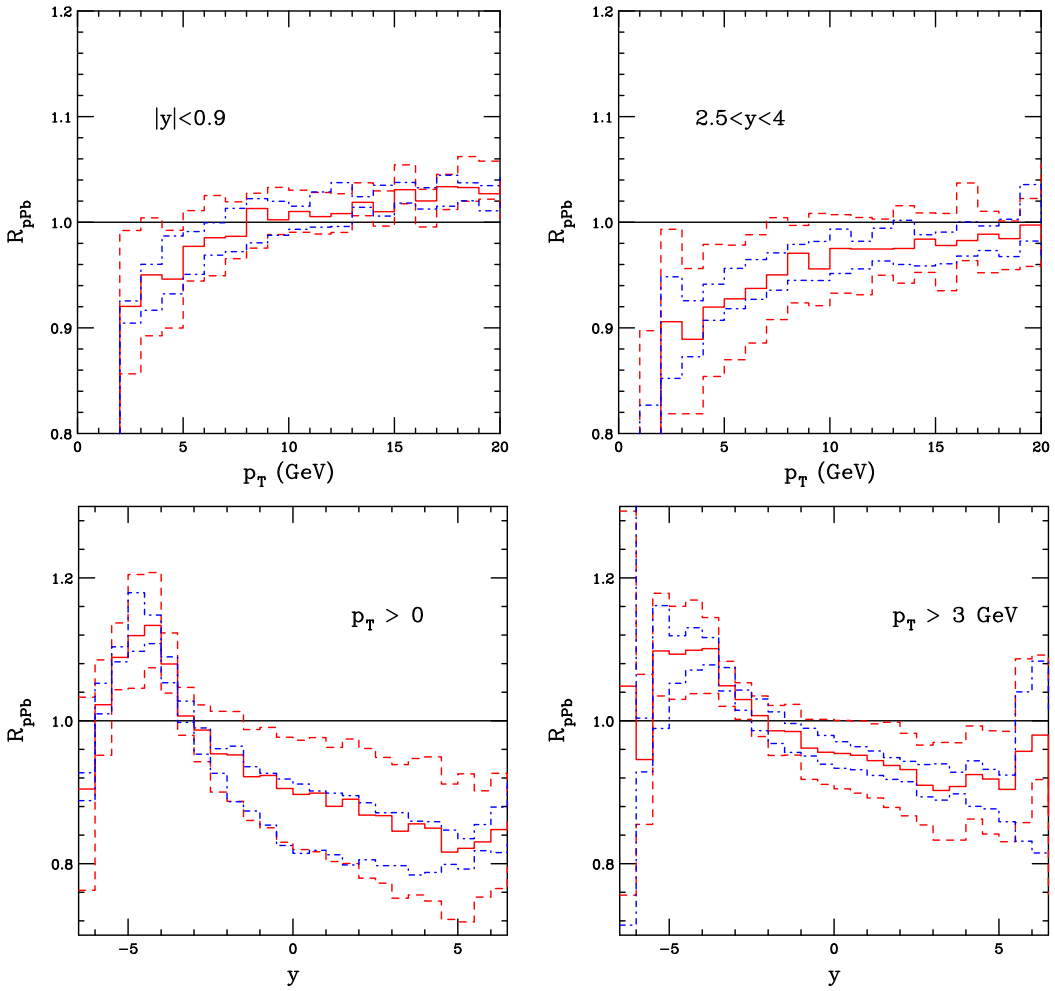

Figure 22: **The $R_{p\mathrm{Pb}}$ ratios for J/ψ as a function of p_T (top) and y (bottom). The dashed red histogram shows the EPS09 uncertainties while the dot-dashed blue histogram shows the dependence on mass and scale. The pp denominator is also calculated at 5 TeV (which isn't available experimentally) and does not take the rapidity shift in pPb into account.**

Gauge Bosons

Cold Matter Effects on W and Z Production

Isospin effects evident for W^+ and W^- production, small effect on Z

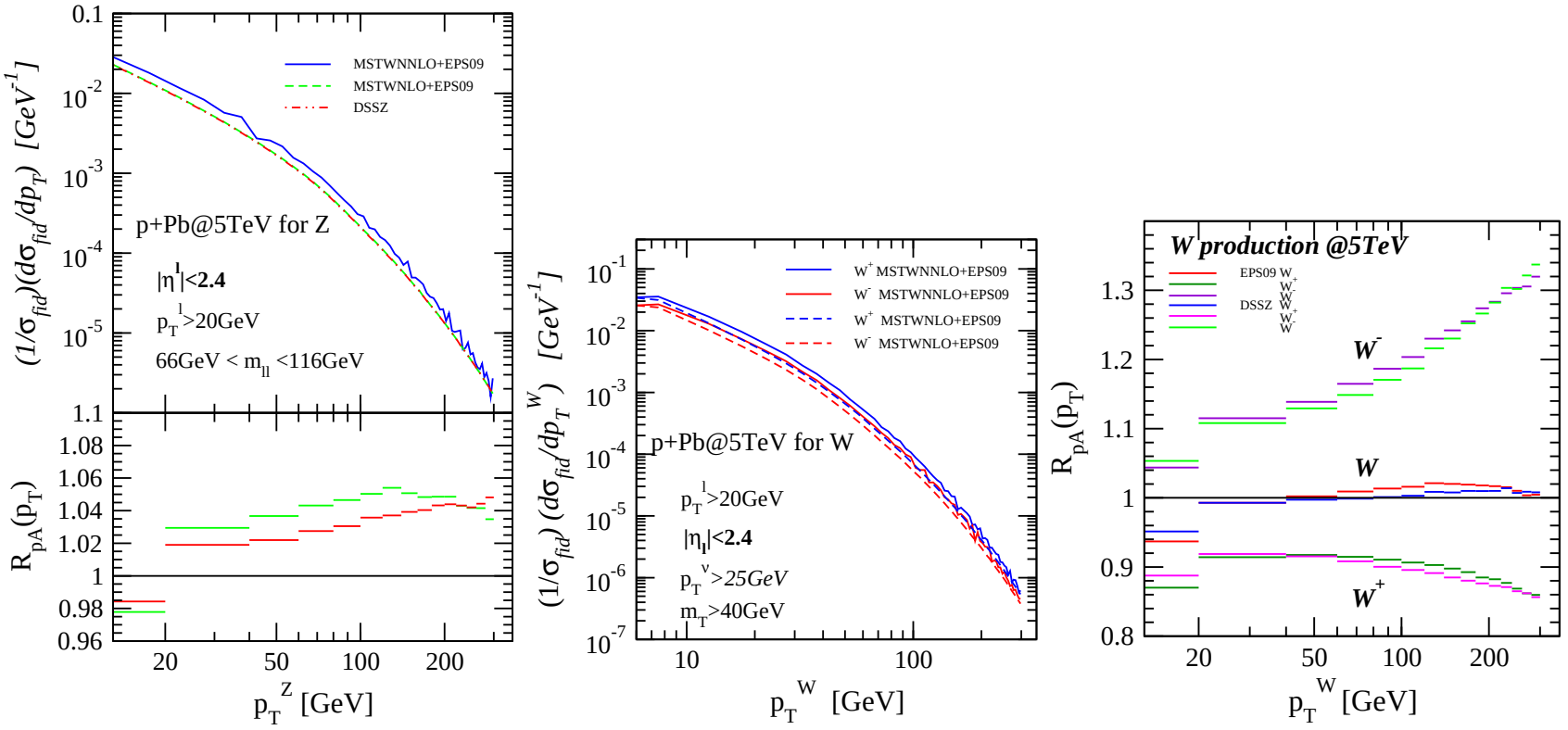

Figure 23: Normalized differential cross section $(1/\sigma_{\rm fid})(d\sigma_{\rm fid}/dp_T^Z)$ for Z (left) and W (center) boson production. In the case of W production, $\sigma_{\rm fid}$ is the sum $W = (W^+ + W^-)$ in the fiducial phase space and p_T^W is the transverse momentum of the W^+ or W^-. The $R_{pA}(p_T)$ for Z is under the cross section on the left side while the value for W, both individually and summed, are shown in the right plot. In both cases, the bin width is 20 GeV. Courtesy of Zhang *et al.*.

Differences in W Charge Asymmetry in pp and p+Pb

Significant difference in W^+ and W^- rapidity distributions due to p+Pb vs pp
Little difference whether calculation is NLO or NNLO

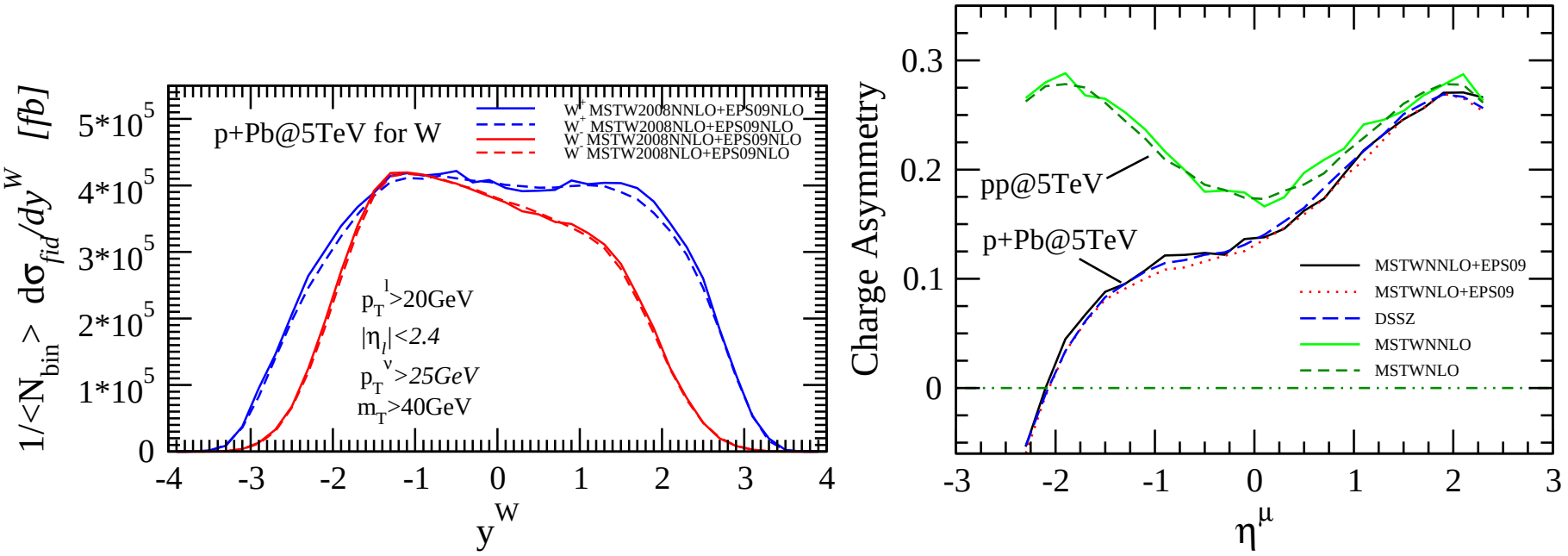

Figure 24: (Left) The W^+ and W^- rapidity distributions. (Right) The charge asymmetry $(N_{W^+} - N_{W^-})/(N_{W^+} + N_{W^-})$ as a function of the charged lepton pseudorapidity for W boson productions in both $p + p$ and $p + Pb$ collisions at 5 TeV. Courtesy of Zhang *et al.*.

Summary

- p+Pb run at LHC will provide interesting studies of cold matter effects in a new energy regime
- These predictions will soon be tested (if they haven't been addressed by the test run)
- Thanks again to everyone who provided predictions